Supporting Information

Ultrafast Tracking of Exciton and Charge Carrier Transport in Optoelectronic Materials on the Nanometer Scale

Christoph Schnedermann[†,a,], Jooyoung Sung[†,a], Raj Pandya[†], Sachin Dev Verma[†], Richard Y. S. Chen[†], Nicolas Gauriot[†], Hope M. Bretscher[†], Philipp Kukura[‡], Akshay Rao[†,*]*

[†]Department of Physics, Cavendish Laboratory, University of Cambridge, JJ Thompson Avenue, Cambridge, CB3 0HE, United Kingdom

[‡]Physical and Theoretical Chemistry Laboratory, University of Oxford, South Parks Road, Oxford OX1 3QZ, United Kingdom

[a] These authors contributed equally to the work.

Contents

1 Pulse characterization

1.1 Spatial characterization of pump pulse

The pump size was determined by recording the fluorescence intensity obtained from sample scanning fluorescent beads (TetraSpeck™ fluorescent microspheres, T7179, diameter ~100 nm) across the pump spot. The retrieved spatial intensity profile was fit to a Gaussian function yielding σ = 115 nm (Figure 1e). This value is close to the expected diffraction limit of σ = 100 nm for a pulse centered at 560 nm and a numerical aperture (NA) of 1.1.

1.2 Temporal characterization

Optical pulses were characterized using a home-built second-harmonic generation frequency-resolved gating (SHG-FROG) setup.[1] Care was taken to match the path lengths in the pulse-characterization arm with the sample stage arm for both pulses. Specifically, pump pulses were focused into the back-aperture of an identical microscope objective by a curved mirror (F = 200 mm) and reflectively collimated (F = 75 mm) before being sent to the SHG-FROG.

The retrieved pulse durations for pump and probe pulses were 9.8 and 6.8 fs, respectively (Figure S1). We remark that the same pump pulses were also compressed without the microscope objective, resulting in a pulse duration of 9.3 fs retrieved via SHG-FROG. Based on the required number of bounces on the chirped mirrors, we can estimate the induced group-velocity dispersion of our microscope objective to be ~1100 fs^2, significantly lower than conventional high-NA multi-component objectives which typically exhibit >4000 fs^2.[2]

In addition to the temporal intensity and phase values, we also report the spectral intensity and phase values retrieved from SHG-FROG in Figure S2. We observe small residual oscillatory phase modulation over the full pulse bandwidth, which can be explained by residual phase oscillation imprinted on the pulses by the employed set of chirped mirrors as well as higher order dispersion effects arising in the setup. This effect prevents compression of our pulses to the transform limit but has only a weak impact on the temporal characteristics, as evident by the near-flat temporal phase (Figure 1c).

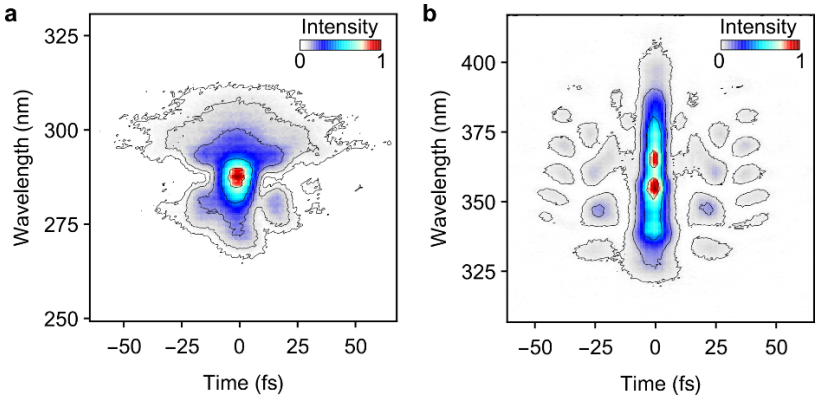

Figure S1. Pulse characterization via second-harmonic generation frequency resolved gating (SHG-FROG). **a**, Pump pulse. **b**, Probe pulse in transmission geometry.

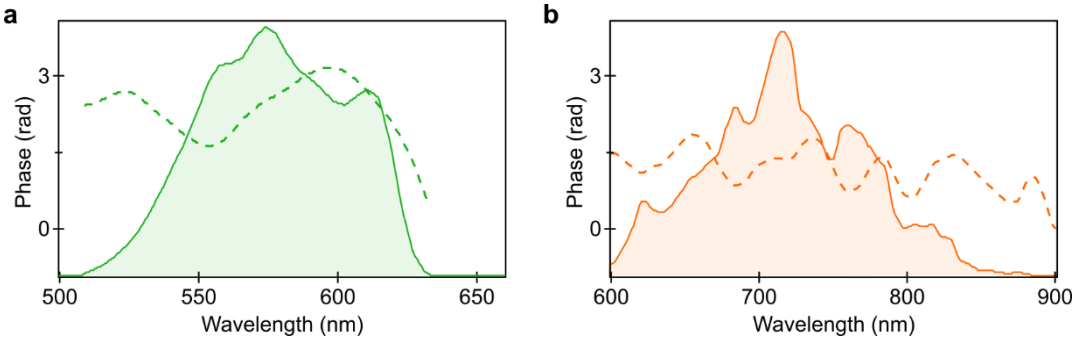

Figure S2. Retrieved spectral intensities (normalized, solid, filled line) and phases (dashed) from second-harmonic generation frequency resolved gating (SHG-FROG). **a**, Pump pulse. **b**, Probe pulse in transmission geometry.

To fully compress the pulses for the employed objects, a more sophisticated pulse-compression scheme based on deformable mirrors or spatial light modulators is necessary.[3]

To estimate the temporal chirp imprinted by the objective and wide-field lens onto a compressed probe pulse, we expanded our imaging path to spectrally-resolve the transient photoresponse from a diffraction-limited section of the image, as outlined in our previous works.[4] By integrating over all space, we can compute a spectrally-resolved transient reflection map (Figure S3a) that highlights a probe chirp of ~700 fs from 670 – 900 nm. This chirp temporally broadens the time resolution to ~50 fs at 740 nm for a 10 nm (full width half maximum) bandpass filter (Figure S3b), but can be improved by employing narrower bandpass filters at the expense of detected photons.

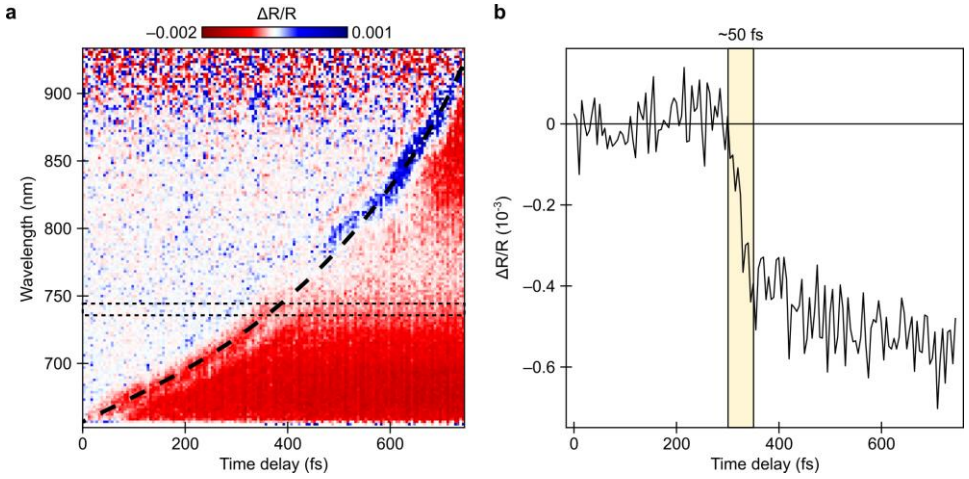

Figure S3. Spectrally-resolved transient reflection microspectroscopy of p-doped Silicon. **a**, Time-resolved map showing the probe chirp (black thick dashed) line for ~700 fs. Spectral distortions in the signal are caused by chromatic aberrations. **b**, Transient kinetics at 740 nm integrated over a full width half maximum of 10 nm (dashed rectangle in **a**), showing a signal rise time of ~50 fs (yellow highlighted area).

We note that the chromatic aberrations of our microscope objective result in spectral distortions induced by phase interference effects native to wide-field imaging in a spectrally-resolved measurement, as evident by the unphysical 'dip' in the transient reflection spectrum in Figure S2a. This effect can be reduced significantly by employing high-NA aberration corrected objectives,[4] which will, however, limit the shortest pump pulse durations that can be achieved.

2 Fit performance

Here, we briefly illustrate the quality of a two-dimensional isotropic Gaussian fit to the pentacene transmission data. The differential point-spread function and the residual of the fitting routine are shown in Figure S4a and S4b, respectively, highlighting a very good representation of the central signal amplitude. The only residual that can be determined above the noise floor stems from diffraction rings associated with the Airy disk point-spread function intrinsic to wide-field detection.

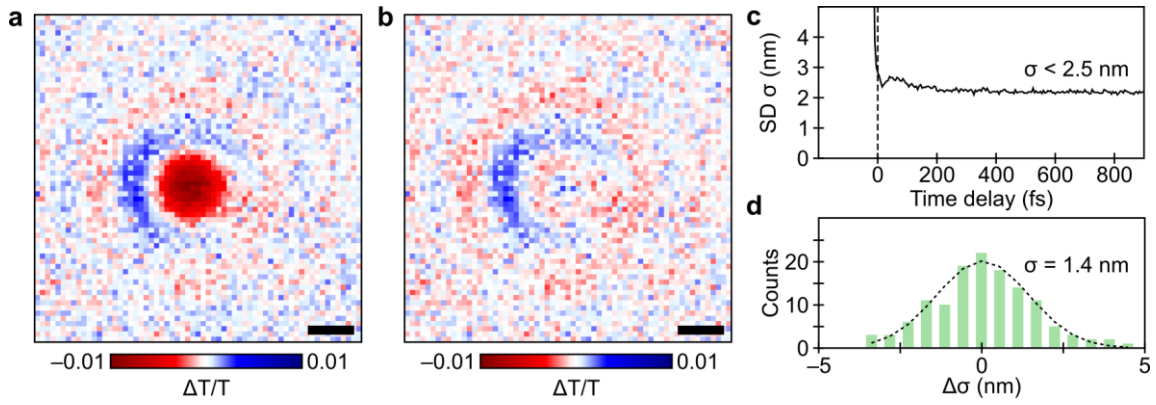

Figure S4. Two-dimensional Gaussian fit performance. **a**, Imaged point-spread function in pentacene at 1 ps. **b**, Residual after subtraction of the fit. Scale bar is 500 nm. **c**, Standard deviation (SD) error on the retrieved Gaussian standard deviation for each recorded time delay. **d**, Histogram of the time-dependent standard deviation fluctuations.

Based on the covariance matrix of the fit, we can derive a standard deviation (SD) error estimate for each retrieved fit coefficient. Of central importance in this work is the standard deviation of the point-spread function, for which we find an SD error of <2.5 nm for all time delays (Figure S4c). This SD error can be compared to the fluctuations in the standard deviation as a function of time, representing signal fluctuations etc. By constructing a histogram of the variation in the standard deviation, we obtain a Gaussian distribution with a SD of σ = 1.4 nm (Figure S4d). An estimate of the overall spatial accuracy can be retrieved by convoluting these two errors, resulting in a total accuracy of ~2.9 nm, sufficient to resolve the 10 nm increase obtained for pentacene in the first 200 fs.

The same approach for p-doped silicon results in a fit SD error of <2.0 nm and an SD fluctuation error of σ = 1.8 nm, resulting in an overall spatial accuracy of ~2.7 nm, again sufficient to resolve the observed growth of ~10 nm (Figure 4b).

Closer inspection of the transient point-spread function (Figure S4a) reveals a slight asymmetry, particularly pronounced in the first positive diffraction ring. To establish if this has an impact on the fit performance, we repeated our spatial fitting procedure using a non-isotropic 2D Gaussian function (Figure S5). We find that the standard deviations along the X and Y dimensions are identical within the noise-level, firmly ruling out a distorted point-spread function. We therefore attribute the observed

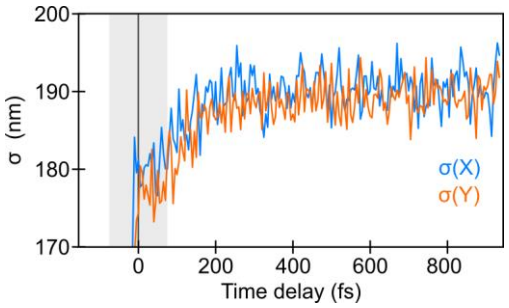

Figure S5. 2D Gaussian fit for each time delayed point-spread function using an anisotropic Gaussian function with independent standard deviations along the X and Y direction of the signal. The grey shaded area represents a time window of potential coherent artefact contributions that is ignored in this work.

asymmetry of the point-spread function to an imperfection in the microscope objective (spherical aberrations), since a re-alignment of the microscope did not significantly change this pattern. Importantly, this effect has no bearings on the central, most intense portion of the point-spread function, allowing for a quantitative analysis, as shown by the invariance of the fitting routine.

3 Sample characterization

3.1 Film preparation and absorption spectrum

Pentacene (99.999%, TCI Chemicals) was thermally evaporated in a custom-built evaporator (Angstrom Engineering) onto cleaned glass substrates (Precision cover glasses thickness No. 1.5H, Marienfeld). The substrates were cleaned by sonication in 9:1 acetone/water solution and subsequently in IPA. Residual impurities were removed by a 10 minute O_2 plasma cleaning process. Thermal evaporation took place at a base pressure below 1×10^{-6} mbar and the deposition rate was maintained at a constant 0.3Å/s using a calibrated quartz crystal microbalance. The absorption spectrum of the final film has the expected spectral shape[5] with a maximum absorbance of 0.5, indicative of a film thickness of ~120 nm (Figure S6).

p-doped Silicon wafers (1% Boron doping, c type, 80 nm SiO_2) were purchased from Graphene Supermarket and cleaned by sonication in a 75:25 vol-% acetone and IPA mixture before use.

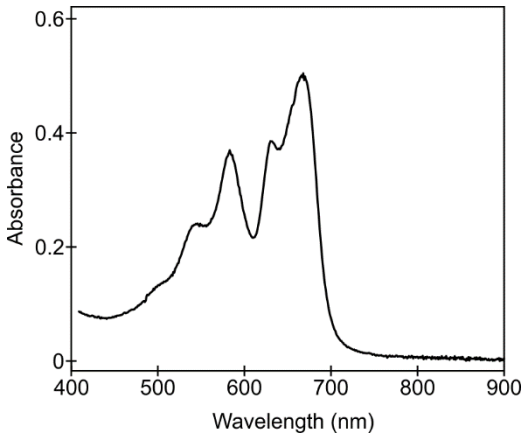

Figure S6. UV-Vis absorption spectrum of pentacene films studied in this work.

3.2 Transient absorption spectroscopy on thin pentacene films

Care has to be taken to avoid spectral overlaps of different transient features in a transient absorption microscope experiment, as different components can exhibit varying carrier density dependencies which can affect the overall recorded transient point-spread function.[6,7] To ensure that the selected probe wavelength of 790 nm is free of these effects and only reports on the photoinduced correlated triplet pair absorption band, we conducted ultrafast transient absorption spectroscopy on the same films that we measured in the microscope. Care was taken to use the same pump pulse as in the microscope (10 fs, 560 nm) to ensure the same excitation properties (Figure S7).[8] The obtained early-time transient absorption spectra match previously published results[5] and allow us to identify the wavelength region > 710 nm to a clean photoinduced transient absorption band, allowing us to assess the spatial dynamics free of artefacts. We remark that the ground-state bleach and stimulated emission bands in pentacene are superimposed at 670 - 690 nm, preventing straightforward microscopic investigations.

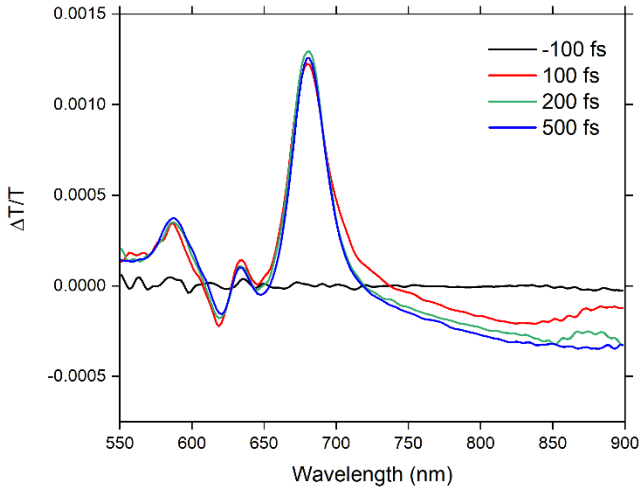

Figure S7. Transient absorption spectroscopy of pentacene thin films measured in the main text at different time delays.

4 Wavelength-dependent ultrafast diffusion in pentacene films

To further verify that spectral overlap can be excluded as a factor causing the ultrafast expansion observed in pentacene, we repeated our transient absorption microscope studies at different probe wavelengths throughout the photoinduced absorption band. As we approach the band edge at 690 nm, spectral overlap of the photoinduced absorption and oppositely-valued stimulated emission and ground state bleach bands is expected to increase. Provided these features have different carrier dependencies, this could result in artificially narrowed point-spread functions, resulting in unphysical diffusion coefficients.

Figure S8 shows the extracted means-square displacement curves for probe wavelengths at 710, 730 and 760 nm. Contrary to the above argument, we observe no significant differences in the spatial expansion between the three wavelengths within our signal-to-noise level and compared to probing the diffusion behavior at 790 nm (Figure 2c). The extracted diffusion coefficients are 158 ± 13, 157 ± 12 and 147 ± 16 $cm^2\ s^{-1}$ at 710, 730 and 760 nm, respectively, comparing well to the retrieved diffusion coefficient of 137 ± 18 $cm^2\ s^{-1}$ at 790 nm. The weak increase in diffusion coefficient might be attributed to an increase in spectral overlaps, but these changes are on the order of the retrieved errors, preventing a definite assignment.

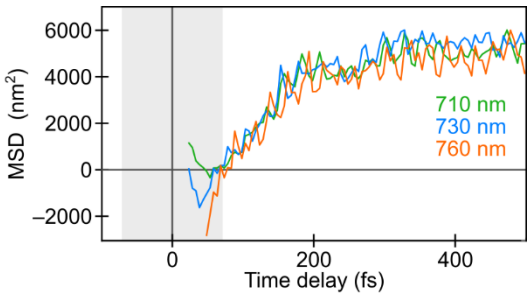

Figure S8. Mean-square displacement traces of pentacene films probed at different wavelengths within the photoinduced triplet pair absorption band.

Combination of transient absorption spectroscopy and wavelength-dependent probing thus suggests an ultrafast band-like transport regime in pentacene during the singlet fission reaction as monitored via the photoinduced triplet pair absorption band.

5 Power dependence of early expansion regime in pentacene films

We investigated the expansion behavior of pentacene for different excitation densities within the linear absorption regime as judged by the power dependence on the differential transmission signal at 1 ps after photoexcitation. Here, we observed no fluence dependence on the diffusion coefficients for different signal levels (Figure S9). We remark that these measurements were carried out on 12 different sample locations. Consequently, morphological changes to the transport behavior cannot be excluded, which manifest in the (non-correlated) spread of the obtained diffusion coefficients as compared to the intrinsic error bar for each measurement.

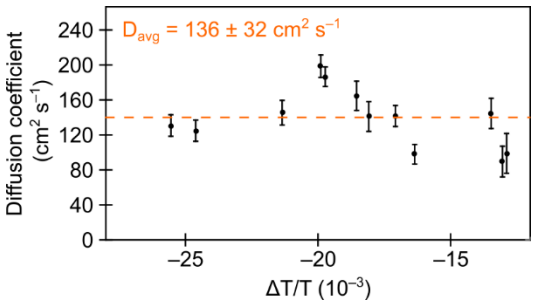

Figure S9. Power dependence of initial diffusion coefficient in pentacene from 75 – 150 fs. The orange dashed line indicates the mean diffusion coefficient (orange) and error bars indicate one standard deviation.

6 References

(1) Trebino, R.; DeLong, K. W.; Fittinghoff, D. N.; Sweetser, J. N.; Krumbügel, M. a.; Richman, B. a.; Kane, D. J. Measuring Ultrashort Laser Pulses in the Time-Frequency Domain Using Frequency-Resolved Optical Gating. *Rev. Sci. Instrum.* **1997**, *68* (9), 3277–3295.

(2) Pawłowska, M.; Goetz, S.; Dreher, C.; Wurdack, M.; Krauss, E.; Razinskas, G.; Geisler, P.; Hecht, B.; Brixner, T. Shaping and Spatiotemporal Characterization of Sub-10-Fs Pulses Focused by a High-NA Objective. *Opt. Express* **2014**, *22* (25), 31496.

(3) Pawłowska, M.; Goetz, S.; Dreher, C.; Wurdack, M.; Krauss, E.; Razinskas, G.; Geisler, P.; Hecht, B.; Brixner, T. Shaping and Spatiotemporal Characterization of Sub-10-Fs Pulses Focused by a High-NA Objective. *Opt. Express* **2014**, *22* (25), 31496.

(4) Schnedermann, C.; Lim, J. M.; Wende, T.; Duarte, A. S.; Ni, L.; Gu, Q.; Sadhanala, A.; Rao, A.; Kukura, P. Sub-10 Fs Time-Resolved Vibronic Optical Microscopy. *J. Phys. Chem. Lett.* **2016**, *7* (23), 4854–4859.

(5) Wilson, M. W. B.; Rao, A.; Clark, J.; Kumar, R. S. S.; Brida, D.; Cerullo, G.; Friend, R. H. Ultrafast Dynamics of Exciton Fission in Polycrystalline Pentacene. *J. Am. Chem. Soc.* **2011**, *133* (31), 11830–11833.

(6) Guo, Z.; Wan, Y.; Yang, M.; Snaider, J.; Zhu, K.; Huang, L. Long-Range Hot-Carrier Transport in Hybrid Perovskites Visualized by Ultrafast Microscopy. *Science (80-.).* **2017**, *356* (6333), 59–62.

(7) Delor, M.; Weaver, H. L.; Yu, Q.; Ginsberg, N. S. Imaging Material Functionality through Three-Dimensional Nanoscale Tracking of Energy Flow. *Nat. Mater.* **2019**.

(8) Pandya, R.; Chen, R. Y. S.; Cheminal, A.; Thomas, T.; Thampi, A.; Tanoh, A.; Richter, J.; Shivanna, R.; Deschler, F.; Schnedermann, C.; et al. Observation of Vibronic-Coupling-Mediated Energy Transfer in Light-Harvesting Nanotubes Stabilized in a Solid-State Matrix. *J. Phys. Chem. Lett.* **2018**, *9* (18), 5604–5611.